Nonorthogonal Multiple Access for Beamforming in Energy-Harvesting Enabled Networks

A. A. Nasir, H. D. Tuan, T. Q. Duong, and M. Debbah

***Abstract*—Wireless power transfer via radio-frequency (RF) radiation is regarded as a potential solution to energize energy-constrained users, who are deployed close to the base stations (near-by users). However, energy transfer requires much more transmit power than normal information transfer, which makes it very challenging to provide the quality of service in terms of throughput for all near-by users and cell-edge users. Thus, it is of practical interest to employ non-orthogonal multiple access (NOMA) to improve the throughput of all network users, while fulfilling the energy harvesting requirements of the near-by users. To realize both energy harvesting and information decoding, we consider a transmit time-switching (transmit-TS) protocol. We formulate two important beamfoming problems of users max-min throughput optimization and energy efficiency maximization under power constraint and energy harvesting thresholds at the nearly-located users. For these problems, the optimization objective and energy harvesting are highly non-convex in beamforming vectors. Thus, we develop efficient path-following algorithms to solve them. In addition, we also consider conventional power splitting (PS)-based energy harvesting receiver. Our numerical results confirm that the proposed transmit-TS based algorithms clearly outperform PS-based algorithms in terms of both, throughput and energy efficiency.**

***Index Terms*—Wireless power transfer, energy harvesting, non-orthogonal multiple access (NOMA), nonconvex optimization, throughput, energy efficiency, quality-of-service (QoS).**

I. Introduction

A. Motivation

To address the energy crisis of enormous wirelessly connected devices, radio frequency (RF) energy harvesting/scavenging has emerged as a potential technology, which converts the energy of the received RF signals into electricity. This can be visualized as an opportunity for wireless communication system to not only deliver information but also energy to the near-by users, the one that are located close to the base station (BS) [1]–[3]. By means of the current state-of-the-art electronics, the received signal cannot be used for energy harvesting and information decoding simultaneously. Thus, to realize both wireless energy harvesting (EH) and information decoding (ID), the user's receivers need to split the received signal for EH and ID either by power splitting (PS) or time switching (TS), where the later-one can be refered to as "receive-TS" [1], [4], [5]. Though the PS approach has been shown to mostly outperform the receive-TS approach, however, the PS is complicated and inefficient for practical implementation. Recent findings in [4], [6] and [7] demonstrate the advantages of new "transmit-TS" approach over PS approach, where information and energy is transferred separately and energy-constrained users' receivers do not need any sophisticated device.

During the information transmission, one of the most critical tasks is to provide quality of service (QoS) in terms of throughput to the users, who are located far from the BS. Non-orthogonal multiple access (NOMA) technique (see e.g. [8] and [9]) is able to improve the throughput at far users by allowing the near-by users to access the information intended for the far users. An efficient beamforming design for NOMA multicell systems has been recently proposed [10].

B. Literature Survey

Very recently, some studies have been made regarding energy harvesting enabled NOMA systems. In [11] and [12], the authors considered a wireless powered communication network, where a BS charges users and enables them to transmit information during uplink communication by using NOMA scheme. Similar study was done by the authors in [13] for wireless-powered sensor network by using a NOMA scheme. In [14], the authors considered a NOMA based heterogeneous network and studied the trade-off among the energy efficiency, fairness, harvested energy, and system sum rate. In [15], the authors designed optimal resource allocation strategies for cognitive radio networks with NOMA. The authors considered non-linear EH model, where secondary users either harvest energy or decode information. The authors in [16] and [17] consider wireless power transfer and NOMA in machine-to-machine communication, where machine-type communication device harvests energy in the downlink while transmits information to BS via machine-type communication gateway in the uplink.

Ali A. Nasir is with the Department of Electrical Engineering, King Fahd University of Petroleum and Minerals (KFUPM), Dhahran, Saudi Arabia (email: anasir@kfupm.edu.sa)

Hoang D. Tuan is with the School of Electrical and Data Engineering, University of Technology, Sydney, NSW 2007, Australia (email: tuan.hoang@uts.edu.au).

Trung Q. Duong is with the School of Electronics, Electrical Engineering and Computer Science, Queen's University Belfast, Belfast BT7 1NN, United Kingdom (e-mail: trung.q.duong@qub.ac.uk).

Merouane Debbah is with the Mathematical and Algorithmic Sciences Laboratory, France Research Center, Huawei Technologies, France (email: merouane.debbah@huawei.com).

In all the above works [11]–[17], the authors assume single antenna nodes and consider a simple power allocation problem. Energy harvesting is more practical with multiple antenna beamforming, however, the above works [11]–[17] do not consider the practical and complex problem of multi-antenna beamforming. In addition, wireless nodes have to either harvest energy or decode information [11]–[13], [15]–[17], and do not need to implement both EH and ID.

In energy harvesting based cooperative NOMA systems, the cell-centered or "nearly-located users" harvest energy from the wireless signals received from the BSs and act as a relay to forward the information to the "far-located users" [18]–[27]. Mostly, authors considered PS approach at the relay users [18]–[25] and showed different analyses, e.g., deriving outage expressions for far end users [18], [19], [21], [23], [25], proposing different selection schemes for users pairing in NOMA [21], optimizing receiver PS ratios and transmit beamforming vectors [22], [24], specifically with the objective of maximizing the data rate of the strong user while satisfying the QoS requirement of the weak user [22], or studying antenna selection schemes at the base station (BS) [25]. Recently, authors in [26] also considered hybrid receive-TS/PS approach for energy harvesting at the relay users. However, it is not practically easy to implement variable range power splitter. In [27], authors considered simple time-switching (TS) mode at the relay receiver, where half of the time is dedicated for energy harvesting.

Exploiting wireless energy harvesting in NOMA systems, authors in [28] considered various energy harvesting protocols, e.g., conventional receive-TS, PS and generalized (hybrid TS/PS), however, they assumed a very simple setup of single antenna BS and single user pair and did not consider multi-antenna beamforming. In [29], the authors also studied wireless power transfer and information transmission in NOMA system, however, they also assumed a simple setup with single antenna BS and employed PS based strategy for energy harvesting.

C. Research Gap and Contribution

Recently, the authors in [22] solve the throughput optimization problem with multi-antenna beamforming and PS based EH in simple NOMA systems with one BS serving one nearly-located user and one far-located user. They employed semidefinite relaxation (SDR) to solve their beamforming-vector optimization problem, which is computationally inefficient as SDR has to first solve for matrix optimization [6], [30]. In addition, the authors in [22] employed a PS-based approach for energy harvesting, which is also not very practical due to the need of variable power splitting. Thus, an efficient solution for such important throughput maximin optimization problem is still missing. Meanwhile, energy efficiency (EE), which is defined as the sum throughput per Joule of consumed energy (ratio of sum throughput to power consumption), is an important key performance indicator for new wireless technologies [31]. Especially, energy harvesting brings in conflicting requirements from the viewpoint of EE, as it requires a stronger transmit power. Thus, energy efficiency maximization is an important research problem in EH enabled NOMA systems. To the best of authors' knowledge, the important problem of energy efficiency maximization with multi-antenna beamforming in EH enabled NOMA network has not been addressed in the literature. It is more difficult to solve the EE maximization problem than the throughput maximization problem due to the additional optimization variables appearing in the denominator of the EE function.

In this article, different from many existing approaches, we consider multi-antenna beamforming in energy harvesting enabled NOMA systems. Moreover, to achieve wireless energy harvesting, we do not prefer PS-based approach because it requires energy to be harvested from information-bearing signal, which needs a sophisticated energy harvesting device with impractical variable power splitter. Keeping in view the need to keep the receiver simple, we propose to consider a "transmit-TS" approach, where information and energy are transmitted separately in fractional times, enabling the energy harvesting by simple devices. Thus, both throughput and harvested energy can be improved by separately designed information and energy beamformers. We formulate two important problems of worst-user throughput maximization and energy efficiency maximization under power constraint and energy harvesting constraints at the nearly-located users. For these problems, the optimization objective and energy harvesting constraints are highly non-convex, thus, we develop efficient path-following algorithms to solve them. For comparison purpose, we consider both PS-based and transmit-TS based energy harvesting and propose novel algorithms to solve above-mentioned novel beamforming problems. Our numerical results confirm that the proposed transmit-TS approach clearly outperforms the PS approach in terms of both, throughput and energy efficiency.

D. Organization and Notation

The paper is organized as follows. After a brief system model, Section II presents the formulation of throughput and EE maximization problems and their computational solution for PS-based NOMA implementation. Section III describes the formulation and solution of such problems for transmit-TS based NOMA implementation. Section IV evaluates the performance of our proposed algorithms by numerical examples. Finally, Section V concludes the paper.

Notation. Bold-faced lower-case letters, e.g., $\mathbf{x}$, are used for vectors and lower-case letters, e.g., x, are used for for scalars. $\mathbf{x}^H$, $\mathbf{x}^T$, and $\mathbf{x}^*$ denote Hermitian transpose, normal transpose, and conjugate of the vector $\mathbf{x}$, respectively. $\|\cdot\|$ stands for the vector's Euclidean norm. $\mathbb{C}$ is the

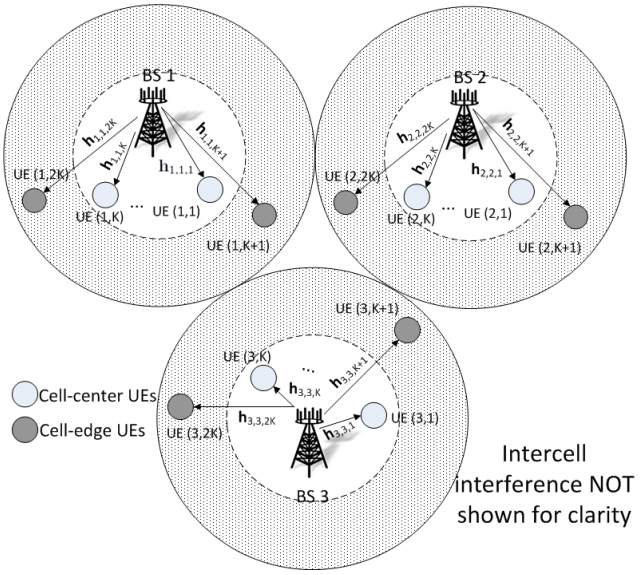

Fig. 1. Downlink multiuser multicell interference scenario in a dense network consisting of K small cells. For clarity, the intercell interference channels are not shown, however, the interference occurs in all K cells.

set of all complex numbers, and $\emptyset$ is an empty set. $\Re\{x\}$ denotes the real part of a complex number x. $\nabla_{\mathbf{x}} f(\mathbf{x})$ is the gradient of function $f(\cdot)$ with respect to its variable $\mathbf{x}$. Also, we define $\langle \mathbf{x}, \mathbf{y} \rangle \triangleq \mathbf{x}^H \mathbf{y}$. $\mathsf{Col}[a]_{i\in\mathcal{I}}$ arranges a_i, $i \in \mathcal{I}$ in row-block. For instance

$$\mathsf{Col}[a]_{i\in\{1,2\}} = \begin{bmatrix} a_1 \\ a_2 \end{bmatrix}.$$

II. System Model and PS-based NOMA

Consider a downlink system consisting of N cells, where the BS of each cell is equipped with N_t antennas to serve $2K$ single-antenna-equipped users (UEs) within its cell. In each cell, there are K near UEs (cell-center UEs), which are located inside the inner circular area and K far UEs (cell-edge UEs), which are located in the ring area between inner circle and outer radius. A representative figure for 3 cells is shown in Fig. 1. The K far UEs in each cell are not only in poorer channel conditions than other K near UEs but also are under more drastic inter-cell interference from adjacent cells.

Upon denoting $\mathcal{I} \triangleq \{1, 2, \cdots, N\}$ and $\mathcal{J} \triangleq \{1, 2, \cdots, 2K\}$, the j-th UE in the i-th cell is referred to as UE $(i, j) \in \mathcal{S} \triangleq \mathcal{I} \times \mathcal{J}$. The cell-center UEs are UE (i, j), $j \in \mathcal{J}_c \triangleq \{1, \cdots, K\}$ while the cell-edge UEs are UE (i, j), $j \in \mathcal{J}_e \triangleq \{K + 1, \cdots, 2K\}$. Thus the set of cell-center UEs and the set of cell-edge UEs are $\mathcal{S}_c \triangleq \mathcal{I} \times \mathcal{J}_c$ and $\mathcal{S}_e \triangleq \mathcal{I} \times \mathcal{J}_e$, respectively. Due their proximity, the cell-center UE (i, j), $j \in \mathcal{J}_c$ is able to do both information decoding and energy harvesting. Due the differentiated channel conditions between the cell-center and cell-edge UEs, each cell-center UE $(i, j) \in \mathcal{S}_c$ is randomly paired with cell-edge UE $(i, p(j)) \in \mathcal{S}_e$ of the same cell to create a virtual cluster to improve the network throughput. [1]

A. PS-based NOMA

For comparison point-of-view with transmit-TS based NOMA (will be presented in Section III), let us first develop the system model, problem formulation, and solution approach for PS-based NOMA implementation.

The signal superpositions are precoded at the BSs prior to being transmitted to the UEs. Specifically, the message intended for UE (i, j) is $s_{i,j} \in \mathbb{C}$ with $\mathbb{E}\{|s_{i,j}|^2\} = 1$, which is beamformed by vector $\mathbf{w}_{i,j} \in \mathbb{C}^{N_t}$. For notational convenience, let us define $\mathbf{w} \triangleq [\mathbf{w}_{i,j}]_{(i,j)\in\mathcal{S}}$. The received signals at UE (i, j) and UE $(i, p(j))$ are expressed as

$$y_{i,j} = \sum_{(s,\ell)\in\mathcal{S}} \mathbf{h}_{s,i,j} \mathbf{w}_{s,\ell} s_{s,\ell} + n_{i,j}, \tag{1}$$

and

$$y_{i,p(j)} = \sum_{(s,\ell)\in\mathcal{S}} \mathbf{h}_{s,i,p(j)} \mathbf{w}_{s,\ell} s_{s,\ell} + n_{i,p(j)} \tag{2}$$

where $\mathbf{h}_{s,i,j} \in \mathbb{C}^{1\times N_t}$ is the MISO channel from the BS $s \in \mathcal{I}$ to UE $(i, j) \in \mathcal{S}$ and $n_{i,j} \sim \mathcal{CN}(0, \sigma^2)$ is the additive noise.

In SWIPT, the power splitter divides the received signal $y_{i,j}$ into two parts in the proportion of $\alpha_{i,j} : (1 - \alpha_{i,j})$, where $\alpha_{i,j} \in (0, 1)$ is termed as the PS ratio for UE (i, j). The first part $\sqrt{\alpha_{i,j}} y_{i,j}$ forms an input to the ID receiver as:

$$\begin{aligned} &\sqrt{\alpha_{i,j}} y_{i,j} + z^c_{i,j} \\ &\quad = \sqrt{\alpha_{i,j}} \left(\sum_{(s,\ell)\in\mathcal{S}} \mathbf{h}_{s,i,j} \mathbf{w}_{s,\ell} s_{s,\ell} + n_{i,j} \right) + z^c_{i,j}, \end{aligned} \tag{3}$$

where $z^c_{i,j} \sim \mathcal{CN}(0, \sigma_c^2)$ is the additional noise introduced by the ID receiver circuitry.

The energy of the second part $\sqrt{1 - \alpha_{i,j}} y_{i,j}$ of the received signal $y_{i,j}$ is harvested by the EH receiver of UE (i, j) as

$$E_{i,j}(\mathbf{w}, \alpha_{i,j}) \triangleq \zeta_{i,j}(1 - \alpha_{i,j}) \left(p_{i,j}(\mathbf{w}) + \sigma^2 \right), \tag{4}$$

where we assume a linear EH model[2]. In (4), the constant $\zeta_{i,j} \in (0, 1)$ denotes the efficiency of energy conversion at the EH receiver, and

$$p_{i,j}(\mathbf{w}) = \sum_{(s,\ell)\in\mathcal{S}} |\mathbf{h}_{s,i,j} \mathbf{w}_{s,\ell}|^2 \tag{5}$$

[1]Using more sophisticated user-pairing strategies may improve the performance of MIMO-NOMA networks (see e.g. [32], [33]) but this is beyond the scope of this paper.

[2]The recently studied non-linear EH model and waveform design for efficient wireless power transfer [34], [35] is beyond the scope of this work, but could be incorporated in future research.

In NOMA, the message $s_{i,p(j)}$ is decoded by UE (i,j) and $(i,p(j))$. The interference plus noise at UE (i,j) in decoding $s_{i,p(j)}$ is

$$\begin{aligned}\mathsf{IN}^c_{i,p(j)}(\mathbf{w}) &\triangleq \alpha_{i,j}\left(\sum_{(s,\ell)\in\mathcal{S}\setminus\{(i,p(j))\}}|\mathbf{h}_{s,i,j}\mathbf{w}_{s,\ell}|^2+\sigma^2\right)\\ &\qquad +\sigma_c^2 \quad (6)\\ &= \alpha_{i,j}(\|\mathcal{L}^c_{i,p(j)}(\mathbf{w})\|^2+\sigma^2)+\sigma_c^2, \quad (7)\end{aligned}$$

with

$$\mathcal{L}^c_{i,p(j)}(\mathbf{w}) \triangleq \mathsf{Col}[\mathbf{h}_{s,i,j}\mathbf{w}_{s,\ell}]_{(s,\ell)\in\mathcal{S}\setminus\{(i,p(j))\}}, \quad (8)$$

which is a linear operator. Therefore, the signal-to-interference-plus-noise (SINR) in decoding $s_{i,p(j)}$ at UE (i,j) is

$$|\mathbf{h}_{i,i,j}\mathbf{w}_{i,p(j)}|^2/\left(\|\mathcal{L}^c_{i,p(j)}(\mathbf{w})\|^2+\sigma^2+\sigma_c^2/\alpha_{i,j}\right)$$

Meanwhile, the edge-user UE $(i,p(j)$ decodes its own message $s_{i,p(j)}$ only, so the interference plus noise at UE $(i,p(j))$ is

$$\begin{aligned}\mathsf{IN}^e_{i,p(j)}(\mathbf{w}) &\triangleq \sum_{(s,\ell)\in\mathcal{S}\setminus\{(i,p(j))\}}|\mathbf{h}_{s,i,p(j)}\mathbf{w}_{s,\ell}|^2+\sigma^2 \quad (9)\\ &= \|\mathcal{L}^e_{i,p(j)}(\mathbf{w})\|^2+\sigma^2 \quad (10)\end{aligned}$$

with

$$\mathcal{L}^e_{i,p(j)}(\mathbf{w}) \triangleq \mathsf{Col}[\mathbf{h}_{s,i,p(j)}\mathbf{w}_{s,\ell}]_{(s,\ell)\in\mathcal{S}\setminus\{(i,p(j))\}}, \quad (11)$$

which is a linear operator.

Suppose that $\mathcal{R}_{i,p(j)}$ is the achievable rate by decoding $s_{i,p(j)}$. Then

$$\begin{aligned}\mathcal{R}_{i,p(j)} &\le \ln\left(1+\frac{|\mathbf{h}_{i,i,j}\mathbf{w}_{i,p(j)}|^2}{\|\mathcal{L}^c_{i,p(j)}(\mathbf{w})\|^2+\sigma^2+\sigma_c^2/\alpha_{i,j}}\right) \quad (12)\\ &\triangleq \psi(\mathbf{h}_{i,i,j}\mathbf{w}_{i,p(j)},\mathcal{L}^c_{i,p(j)}(\mathbf{w}),\alpha_{i,j}), \quad (13)\end{aligned}$$

$$\begin{aligned}\mathcal{R}_{i,p(j)} &\le \ln\left(1+\frac{|\mathbf{h}_{i,i,p(j)}\mathbf{w}_{i,p(j)}|^2}{\|\mathcal{L}^e_{i,p(j)}(\mathbf{w})\|^2+\sigma^2}\right) \quad (14)\\ &\triangleq \psi(\mathbf{h}_{i,i,j}\mathbf{w}_{i,p(j)},\mathcal{L}^e_{i,p(j)}(\mathbf{w}),0), \quad (15)\end{aligned}$$

UE (i,j) subtracts $s_{i,p(j)}$ from the right hand side of (3) in decoding $s_{i,j}$. Then the achievable rate $\mathcal{R}_{i,j}$ by decoding $s_{i,j}$ is

$$\begin{aligned}\mathcal{R}_{i,j} &\le \ln\left(1+\frac{|\mathbf{h}_{i,i,j}\mathbf{w}_{i,j}|^2}{\|\mathcal{L}^c_{i,j}(\mathbf{w})\|^2+\sigma^2+\sigma_c^2/\alpha_{i,j}}\right) \quad (16)\\ &\triangleq \psi(\mathbf{h}_{i,i,j}\mathbf{w}_{i,j},\mathcal{L}_{i,j}(\mathbf{w}),\alpha_{i,j}), \quad (17)\end{aligned}$$

where the general rate function $\psi(\mathbf{x},\mathbf{y},\nu)$ is given by

$$\psi(\mathbf{x},\mathbf{y},\nu)=\begin{cases}\ln\left(1+\frac{\|\mathbf{x}\|^2}{\|\mathbf{y}\|^2+\sigma^2+\sigma_c^2/\nu}\right) & \text{for} \quad \nu>0\\ \ln\left(1+\frac{\|\mathbf{x}\|^2}{\|\mathbf{y}\|^2+\sigma^2}\right) & \text{for} \quad \nu=0\end{cases} \quad (18)$$

and

$$\mathcal{L}^c_{i,j}(\mathbf{w}) \triangleq \mathsf{Col}[\mathbf{h}_{s,i,j}\mathbf{w}_{s,\ell}]_{(s,\ell)\in\mathcal{S}\setminus\{(i,p(j)),(i,j)\}}.$$

For convenience, we also use the notations

$$\boldsymbol{\alpha}\triangleq(\alpha_{i,j})_{(i,j)\in\mathcal{S}}, \boldsymbol{\alpha}^{(\kappa)}\triangleq(\alpha^{(\kappa)}_{i,j})_{(i,j)\in\mathcal{S}}.$$

We consider two basic problems:

1) *Throughput maximin optimization*

$$\max_{\mathbf{w},\mathcal{R},\boldsymbol{\alpha}} \min_{(i,j)\in\mathcal{I}\times\mathcal{J}} \mathcal{R}_{i,j} \quad \text{s.t.} \quad (12),(14),(16), \quad (19a)$$

$$\zeta_{i,j}\left(p_{i,j}(\mathbf{w})+\sigma^2\right)\ge\frac{e^{\min}_{i,j}}{1-\alpha_{i,j}}, i\in\mathcal{I}, j\in\mathcal{J}_c, \quad (19b)$$

$$0<\alpha_{i,j}<1, i\in\mathcal{I}, j\in\mathcal{J}_c, \quad (19c)$$

$$\sum_{j\in\mathcal{J}}\|\mathbf{w}_{i,j}\|^2\le P_i^{\max},\ \forall i\in\mathcal{I} \quad (19d)$$

where (19a) defines the EH constraint such that $e^{\min}_{i,j}$ is the EH threshold and $p_{i,j}(\mathbf{w})$ is defined in (5), $P_i^{\max}$ in (19d) is the transmit power budget of BS i, and $\mathcal{R}\triangleq[\mathcal{R}_{i,j}]_{(i,j)\in\mathcal{I}\times\mathcal{J}}$.

2) *Energy-efficiency maximization under QoS constraints*

$$\max_{\mathbf{w},\mathcal{R}} \mathcal{F}(\mathbf{w},\mathcal{R})\triangleq\frac{\sum_{(i,j)\in\mathcal{I}\times\mathcal{J}}\mathcal{R}_{i,j}}{\pi(\mathbf{w})+P_c}$$

$$\text{s.t.} \quad (12),(14),(16),(19b),(19c),(19d) \quad (20a)$$

$$\mathcal{R}_{i,j}\ge r_{i,j},\ \forall i\in\mathcal{I},\ \forall j\in\mathcal{J}_c, \quad (20b)$$

$$\mathcal{R}_{i,p(j)}\ge r_{i,p(j)}, \forall i\in\mathcal{I}, \forall j\in\mathcal{J}_c, \quad (20c)$$

where $\pi(\mathbf{w})=\sum_{i\in\mathcal{I}}\sum_{j\in\mathcal{J}}\|\mathbf{w}_{i,j}\|^2$, P_c is the circuit power for each transmission, and (20b) and (20c) are the quality-of-service constraints, such that, $r_{i,j}$, $\forall i\in\mathcal{I}$, $\forall j\in\mathcal{J}$ is the threshold rate to ensure a certain quality-of-service.

B. Computational solutions for PS-based NOMA

Let us first address the throughput maximin optimization problem (19). We have to resolve the non-convex rate constraints (12), (14), and (16) and the non-convex EH constraint (19b). In order to deal with the non-convexity of rate constraints (12), (14), and (16), we have to provide a concave lower bounding function for $\psi(\mathbf{x},\mathbf{y},0)$ defined by (18), at a given point $(\mathbf{x}^{(\kappa)},\mathbf{y}^{(\kappa)})$ [5], [7]. In the Appendix A, we prove the following new and universal bound:

$$\begin{aligned}\psi(\mathbf{x},\mathbf{y},0) &\ge \Lambda_0(\mathbf{x},\mathbf{y}) \quad (21)\\ &\triangleq a_0(\mathbf{x}^{(\kappa)},\mathbf{y}^{(\kappa)})-\frac{\|\mathbf{x}^{(\kappa)}\|^2}{2\Re\{(\mathbf{x}^{(\kappa)})^H\mathbf{x}\}-\|\mathbf{x}^{(\kappa)}\|^2}\\ &\quad -b_0(\mathbf{x}^{(\kappa)},\mathbf{y}^{(\kappa)})\|\mathbf{x}\|^2-c_0(\mathbf{x}^{(\kappa)},\mathbf{y}^{(\kappa)})\|\mathbf{y}\|^2, \quad (22)\end{aligned}$$

over the trust region

$$2\Re\{(\mathbf{x}^{(\kappa)})^H\mathbf{x}\}-\|\mathbf{x}^{(\kappa)}\|^2>0, \quad (23)$$

and

$$\psi(\mathbf{x}^{(\kappa)},\mathbf{y}^{(\kappa)},0)=\Lambda_0(\mathbf{x}^{(\kappa)},\mathbf{y}^{(\kappa)}) \tag{24}$$

where

$$a_0(\mathbf{x}^{(\kappa)},\mathbf{y}^{(\kappa)})=\psi(\mathbf{x}^{(\kappa)},\mathbf{y}^{(\kappa)})+2 - \frac{\|\mathbf{x}^{(\kappa)}\|^2}{(\|\mathbf{x}^{(\kappa)}\|^2+\|\mathbf{y}^{(\kappa)}\|^2+\sigma^2)}\frac{\sigma^2}{\|\mathbf{y}^{(\kappa)}\|^2+\sigma^2}, \tag{25}$$

$$b_0(\mathbf{x}^{(\kappa)},\mathbf{y}^{(\kappa)})=\frac{\|\mathbf{y}^{(\kappa)}\|^2+\sigma^2}{(\|\mathbf{x}^{(\kappa)}\|^2+\|\mathbf{y}^{(\kappa)}\|^2+\sigma^2)\|\mathbf{x}^{(\kappa)}\|^2} > 0, \tag{26}$$

$$c_0(\mathbf{x}^{(\kappa)},\mathbf{y}^{(\kappa)})=\frac{\|\mathbf{x}^{(\kappa)}\|^2}{(\|\mathbf{x}^{(\kappa)}\|^2+\|\mathbf{y}^{(\kappa)}\|^2+\sigma^2)(\|\mathbf{y}^{(\kappa)}\|^2+\sigma^2)} > 0. \tag{27}$$

Analogously,

$$\psi(\mathbf{x},\mathbf{y},\mu)\geq\Lambda(\mathbf{x},\mathbf{y},\mu) \tag{28}$$

$$\triangleq a(\mathbf{x}^{(\kappa)},\mathbf{y}^{(\kappa)},\mu^{(\kappa)}) - \frac{\|\mathbf{x}^{(\kappa)}\|^2}{2\Re\{(\mathbf{x}^{(\kappa)})^H\mathbf{x}\}-\|\mathbf{x}^{(\kappa)}\|^2} - b(\mathbf{x}^{(\kappa)},\mathbf{y}^{(\kappa)},\mu^{(\kappa)})\|\mathbf{x}\|^2 - c(\mathbf{x}^{(\kappa)},\mathbf{y}^{(\kappa)},\mu^{(\kappa)})(\|\mathbf{y}\|^2+\sigma_c^2/\mu), \tag{29}$$

over the trust region (23) and

$$\psi(\mathbf{x}^{(\kappa)},\mathbf{y}^{(\kappa)},\mu^{(\kappa)})=\Lambda(\mathbf{x}^{(\kappa)},\mathbf{y}^{(\kappa)},\mu^{(\kappa)}) \tag{30}$$

where

$$a(\mathbf{x}^{(\kappa)},\mathbf{y}^{(\kappa)},\mu^{(\kappa)})=\psi(\mathbf{x}^{(\kappa)},\mathbf{y}^{(\kappa)},\mu^{(\kappa)})+2 - \frac{\|\mathbf{x}^{(\kappa)}\|^2}{\|\mathbf{x}^{(\kappa)}\|^2+\|\mathbf{y}^{(\kappa)}\|^2+\sigma^2+\sigma_c^2/\mu^{(\kappa)}} \times\frac{\sigma^2}{\|\mathbf{y}^{(\kappa)}\|^2+\sigma^2+\sigma_c^2/\mu^{(\kappa)}}, \tag{31}$$

$$0<b(\mathbf{x}^{(\kappa)},\mathbf{y}^{(\kappa)},\mu^{(\kappa)}) =\frac{\|\mathbf{y}^{(\kappa)}\|^2+\sigma^2+\sigma_c^2/\mu^{(\kappa)}}{(\|\mathbf{x}^{(\kappa)}\|^2+\|\mathbf{y}^{(\kappa)}\|^2+\sigma^2+\sigma_c^2/\mu^{(\kappa)})\|\mathbf{x}^{(\kappa)}\|^2}, \tag{32}$$

$$0<c(\mathbf{x}^{(\kappa)},\mathbf{y}^{(\kappa)},\mu^{(\kappa)}) =\frac{\|\mathbf{x}^{(\kappa)}\|^2}{\left(\|\mathbf{x}^{(\kappa)}\|^2+\|\mathbf{y}^{(\kappa)}\|^2+\sigma^2+\frac{\sigma_c^2}{\mu^{(\kappa)}}\right)\left(\|\mathbf{y}^{(\kappa)}\|^2+\sigma^2+\frac{\sigma_c^2}{\mu^{(\kappa)}}\right)}. \tag{33}$$

Next, we can find an inner convex approximation for the EH constraint, given by cf. (35b), by using the following approximation [7]

$$|\mathbf{h}_{s,i,j}^H\mathbf{w}_{s,\ell}|^2\geq-|\mathbf{h}_{s,i,j}^H\mathbf{w}_{s,\ell}^{(\kappa)}|^2 + 2\Re\left\{\left(\mathbf{w}_{s,\ell}^{(\kappa)}\right)^H\mathbf{h}_{s,i,j}\mathbf{h}_{s,i,j}^H\mathbf{w}_{s,\ell}\right\},\ \forall\mathbf{w}_{s,\ell},\mathbf{w}_{s,\ell}^{(\kappa)} \tag{34}$$

Therefore, initialized by a feasible point $(\mathbf{w}^{(0)},\boldsymbol{\alpha}^{(0)})$, at the κ-th iteration we solve the following convex quadratic optimization problem to generate the next feasible point $(\mathbf{w}^{(\kappa+1)},\boldsymbol{\alpha}^{(\kappa+1)})$:

$$\max_{\mathbf{w},\boldsymbol{\alpha},\mathcal{R}_{i,j}}\ \min_{(i,j)\in\mathcal{I}\times\mathcal{J}}\ \mathcal{R}_{i,j}\quad\text{s.t.}\quad(19c),(19d) \tag{35a}$$

$$\zeta_{i,j}\sum_{(s,\ell)\in\mathcal{S}}\left(2\Re\{(\mathbf{w}_{s,\ell}^{(\kappa)})^H\mathbf{h}_{s,i,j}^H\mathbf{h}_{s,i,j}\mathbf{w}_{s,l}\}-|\mathbf{h}_{s,i,j}\mathbf{w}_{s,l}^{(\kappa)}|^2\right) + \zeta_{i,j}\sigma^2\geq\frac{e_{i,j}^{\min}}{1-\alpha_{i,j}}, \tag{35b}$$

$$\mathcal{R}_{i,p(j)}\leq\Lambda(\mathbf{h}_{i,i,j}\mathbf{w}_{i,p(j)},\mathcal{L}_{i,p(j)}^c(\mathbf{w}),\alpha_{i,j}), \tag{35c}$$

$$\mathcal{R}_{i,p(j)}\leq\Lambda_0(\mathbf{h}_{i,i,p(j)}\mathbf{w}_{i,p(j)},\mathcal{L}_{i,p(j)}^e(\mathbf{w})), \tag{35d}$$

$$\mathcal{R}_{i,j}\leq\Lambda(\mathbf{h}_{i,i,j}\mathbf{w}_{i,j},\mathcal{L}_{i,j}^c(\mathbf{w}),\alpha_{i,j}), \tag{35e}$$

$$2\Re\{(\mathbf{w}_{i,p(j)}^{(\kappa)})^H\mathbf{h}_{i,i,p(j)}^H\mathbf{h}_{i,i,p(j)}\mathbf{w}_{i,p(j)}\} - \|\mathbf{h}_{i,i,p(j)}\mathbf{w}_{i,p(j)}^{(\kappa)}\|^2>0, \tag{35f}$$

$$2\Re\{(\mathbf{w}_{i,p(j)}^{(\kappa)})^H\mathbf{h}_{i,i,j}^H\mathbf{h}_{i,i,j}\mathbf{w}_{i,p(j)}\}-\|\mathbf{h}_{i,i,j}\mathbf{w}_{i,p(j)}^{(\kappa)}\|^2>0, \tag{35g}$$

$$2\Re\{(\mathbf{w}_{i,j}^{(\kappa)})^H\mathbf{h}_{i,i,j}^H\mathbf{h}_{i,i,j}\mathbf{w}_{i,j}\}-\|\mathbf{h}_{i,i,j}\mathbf{w}_{i,j}^{(\kappa)}\|^2>0, \tag{35h}$$

$$\forall\quad(i,j)\in\mathcal{I}\times\mathcal{J}_c.$$

Algorithm 1 PS-based algorithm for throughput max-min optimization problem (19)

Initialization: Set $\kappa:=0$ and a feasible point $\mathbf{w}^{(0)}$ for constraints (19b), (19c), (19d).

1: **repeat**
2: Solve the convex optimization problem (35) to obtain the optimal solution $\mathbf{w}^{(\kappa+1)}$.
3: Set $\kappa:=\kappa+1$.
4: **until** Convergence

Algorithm 1 outlines the steps to solve the throughput maximin optimization problem (19). By using similar arguments to that shown in [5], [6], we can easily show that Algorithm 1 converges to a Karush-Kuhn-Tucker (KKT) point of (19). The initialization procedure will be stated shortly.

Next, we address the energy-efficiency maximization problem (20), which is equivalent to the following minimization problem

$$\min_{\mathbf{w},\boldsymbol{\alpha},\mathcal{R}}\ \frac{\pi(\mathbf{w})+P_c}{\sum_{(i,j)\in\mathcal{I}\times\mathcal{J}}\mathcal{R}_{i,j}} \quad\text{s.t.}\quad(12),(14),(16),(19b),(19c),(19d),(20b),(20c). \tag{36}$$

The advantage of this transformation is that the objective function is already convex so there is no need of using Dinkelbach's iteration or approximating it. Actually, the Dinkelbach iteration for (20) still involves a nonconvex optimization problem, which is as computationally difficult as (20) itself (see e.g., [36]). Initialized by a feasible point $(\mathbf{w}^{(0)},\boldsymbol{\alpha}^{(0)})$, at the κ-th iteration we solve the following

Algorithm 2 PS-based algorithm for energy-efficiency (EE) maximization problem (20)

Initialization: Set $\kappa := 0$ and a feasible point $\mathbf{w}^{(0)}$ for constraints (19d), (20b)-(20c).

1: **repeat**
2: Solve the convex optimization problem (37) to obtain the optimal solution $\mathbf{w}^{(\kappa+1)}$.
3: Set $\kappa := \kappa + 1$.
4: **until** Convergence

convex optimization problem to generate its next feasible point $(\mathbf{w}^{(\kappa+1)}, \boldsymbol{\alpha}^{(\kappa+1)})$:

$$\min_{\mathbf{w},\boldsymbol{\alpha},\mathcal{R}} \frac{\pi(\mathbf{w}) + P_c}{\sum_{(i,j)\in\mathcal{I}\times\mathcal{J}} \mathcal{R}_{i,j}} \quad \text{s.t.} \quad (19c), (19d), (20b), (20c), (35b) - (35h). \quad (37)$$

Algorithm 2 outlines the steps to solve the PS-based algorithm for energy-efficiency (EE) maximization problem (20).

Generation of the initial points: A feasible point for initializing Algorithm 2 is found via iterations

$$\max_{\mathbf{w},\mathcal{R}} \min_{(i,j)\in\mathcal{I}\times\mathcal{J}_c} \left\{ \frac{\mathcal{R}_{i,j}}{r_{i,j}} - 1, \frac{\mathcal{R}_{i,p(j)}}{r_{i,p(j)}} - 1, \right.$$
$$\left. \zeta_{i,j} \sum_{(s,\ell)\in\mathcal{S}} \left(2\Re\{(\mathbf{w}_{s,\ell}^{(\kappa)})^H \mathbf{h}_{s,i,j}^H \mathbf{h}_{s,i,j} \mathbf{w}_{s,l}\} - |\mathbf{h}_{s,i,j}\mathbf{w}_{s,l}^{(\kappa)}|^2\right) + \zeta_{i,j}\sigma^2 - \frac{e_{i,j}^{\min}}{1-\alpha_{i,j}} \right\}$$
$$\text{s.t.} \quad (19c), (19d), (35c) - (35h) \quad (38)$$

till reaching a value more than or equal to 0.

A good feasible point for initializing Algorithm 1 is also found from (38), however, by considering only the third factor inside the max-min objective.

III. Transmit TS-based NOMA

In a time-switching (TS) based system, a fraction of time $0 < \rho < 1$ is used for power transfer while the remaining fraction of time $1-\rho$ for information transfer, where ρ is termed as TS ratio. For power transfer, we have to design beamforming vectors $\mathbf{w}_{i,j}^E$, $\forall$, $i \in \mathcal{I}$, $j \in \mathcal{J}_c$, thus, the harvested energy by the cell-center user UE(i,j) is expressed as

$$E_{i,j}(\mathbf{w}^E, \rho) \triangleq \rho\zeta_{i,j}(p_{i,j}(\mathbf{w}^E) + \sigma^2), \quad (39)$$
$$p_{i,j}(\mathbf{w}^E) = \sum_{(s,\ell)\in\mathcal{S}_c} |\mathbf{h}_{s,i,j}\mathbf{w}_{s,\ell}^E|^2$$

and $\zeta_{i,j} \in (0,1)$ is the energy conversion efficiency for the EH receiver. Here, we assume a common TS ratio ρ for all BSs, $i \in \mathcal{I}$, where near-by users harvest energy through wireless signals not only from the serving BSs but also from the neighboring BSs. Note that the harvested and stored energy $E_{i,j}$ may be used later for different power constrained operations at cell-center UEs (i,j), e.g., assisting uplink data transmission to the BS or performing downlink information processing. Let us denote $\mathbf{w}^E \triangleq [\mathbf{w}_{i,j}^E]_{i\in\mathcal{I},j\in\mathcal{J}_c}$.

The remaining time $(1-\rho)$ will be used for information decoding by all users UE (i,j), $i \in \mathcal{I}, j \in \mathcal{J}$. Let $\mathbf{w}^I \triangleq [\mathbf{w}_{i,j}^I]_{i\in\mathcal{I},j\in\mathcal{J}}$ define the information beamforming vectors and suppose that $\mathcal{R}_{i,p(j)}$ is the achievable rate by decoding $s_{i,p(j)}$. Then

$$\mathcal{R}_{i,p(j)} \leq (1-\rho)\ln\left(1 + \frac{|\mathbf{h}_{i,i,j}\mathbf{w}_{i,p(j)}^I|^2}{\|\mathcal{L}_{i,p(j)}^c(\mathbf{w}^I)\|^2 + \sigma^2}\right) \quad (40)$$

$$\mathcal{R}_{i,p(j)} \leq (1-\rho)\ln\left(1 + \frac{|\mathbf{h}_{i,i,p(j)}\mathbf{w}_{i,p(j)}^I|^2}{[\mathcal{L}_{i,p(j)}^e(\mathbf{w}^I)]^2 + \sigma^2}\right) \quad (41)$$

After decoding $s_{i,p(j)}$, UE (i,j), $j \in \mathcal{J}_c$ decodes $s_{i,j}$. Then the achievable rate $\mathcal{R}_{i,j}$ by decoding $s_{i,j}$ is

$$\mathcal{R}_{i,j} \leq (1-\rho)\ln\left(1 + \frac{|\mathbf{h}_{i,i,j}\mathbf{w}_{i,j}^I|^2}{\|\mathcal{L}_{i,j}^c(\mathbf{w}^I)\|^2 + \sigma^2}\right) \quad (42)$$

Rewrite (40)-(42) by

$$\frac{\mathcal{R}_{i,p(j)}}{1-\rho} \leq \ln\left(1 + \frac{|\mathbf{h}_{i,i,j}\mathbf{w}_{i,p(j)}^I|^2}{\|\mathcal{L}_{i,p(j)}^c(\mathbf{w}^I)\|^2 + \sigma^2}\right) \quad (43)$$

$$\frac{\mathcal{R}_{i,p(j)}}{1-\rho} \leq \ln\left(1 + \frac{|\mathbf{h}_{i,i,p(j)}\mathbf{w}_{i,p(j)}^I|^2}{[\mathcal{L}_{i,p(j)}^e(\mathbf{w}^I)]^2 + \sigma^2}\right) \quad (44)$$

and

$$\frac{\mathcal{R}_{i,j}}{1-\rho} \leq \ln\left(1 + \frac{|\mathbf{h}_{i,i,j}\mathbf{w}_{i,j}^I|^2}{\|\mathcal{L}_{i,j}^c(\mathbf{w}^I)\|^2 + \sigma^2}\right) \quad (45)$$

Thus, throughput maximin optimization problem for TS-based NOMA SWIPT system is given by

$$\max_{\mathbf{w}^I,\mathbf{w}^E,\mathcal{R},\rho} \min_{(i,j)\in\mathcal{I}\times\mathcal{J}} \mathcal{R}_{i,j} \quad \text{s.t.} \quad (43), (44), (45), \quad (46a)$$
$$\zeta_{i,j}\left(p_{i,j}(\mathbf{w}^E) + \sigma^2\right) \geq \frac{e_{i,j}^{\min}}{\rho}, i \in \mathcal{I}, j \in \mathcal{J}_c, \quad (46b)$$
$$0 < \rho < 1, \quad (46c)$$
$$\frac{1}{1-\rho}\sum_{j\in\mathcal{J}_c} \|\mathbf{w}_{i,j}^E\|^2 + \sum_{j\in\mathcal{J}} \|\mathbf{w}_{i,j}^I\|^2 \leq \frac{P_i^{\max}}{1-\rho} + \sum_{j\in\mathcal{J}_c} \|\mathbf{w}_{i,j}^E\|^2, \ \forall i \in \mathcal{I} \quad (46d)$$
$$\|\mathbf{w}_{i,j}^E\|^2 \leq P_i^{\max} \ \forall i \in \mathcal{I}, j \in \mathcal{J}_c \quad (46e)$$
$$\|\mathbf{w}_{i,j}^I\|^2 \leq P_i^{\max} \ \forall i \in \mathcal{I}, j \in \mathcal{J}. \quad (46f)$$

Note that the power constraint (46d) is the equivalent reexpression of the sum power constraint

$$\rho\sum_{j\in\mathcal{J}_c} \|\mathbf{w}_{i,j}^E\|^2 + (1-\rho)\sum_{j\in\mathcal{J}} \|\mathbf{w}_{i,j}^I\|^2 \leq P_i^{\max}, \ \forall i \in \mathcal{I}.$$

By using the approximation of a linear variable with a quadratic one [37, (78)] and the new bounds derived in

Appendix A, we innerly approximate (43), (44) and (45), at the κ-th iteration, by

$$0.5\frac{\frac{(\mathcal{R}_{i,p(j)})^2}{\mathcal{R}_{i,p(j)}^{(\kappa)}}+\mathcal{R}_{i,p(j)}^{(\kappa)}}{1-\rho} \leq \quad \Lambda_0(\mathbf{h}_{i,i,j}\mathbf{w}_{i,p(j)}^I, \mathcal{L}_{i,p(j)}^c(\mathbf{w}^I)), \tag{47}$$

$$0.5\frac{\frac{(\mathcal{R}_{i,p(j)})^2}{\mathcal{R}_{i,p(j)}^{(\kappa)}}+\mathcal{R}_{i,p(j)}^{(\kappa)}}{1-\rho} \leq \quad \Lambda_0(\mathbf{h}_{i,i,p(j)}\mathbf{w}_{i,p(j)}^I, \mathcal{L}_{i,p(j)}^e(\mathbf{w}^I)) \tag{48}$$

and

$$0.5\frac{\frac{(\mathcal{R}_{i,j})^2}{\mathcal{R}_{i,j}^{(\kappa)}}+\mathcal{R}_{i,j}^{(\kappa)}}{1-\rho} \leq \quad \Lambda_0(\mathbf{h}_{i,i,j}\mathbf{w}_{i,j}^I, \mathcal{L}_{i,j}^c(\mathbf{w}^I)) \tag{49}$$

over the trust regions

$$\begin{aligned} &2\Re\{(\mathbf{w}_{i,p(j)}^{I,(\kappa)})^H\mathbf{h}_{i,i,p(j)}^H\mathbf{h}_{i,i,p(j)}\mathbf{w}_{i,p(j)}^I\} \\ &\quad -\|\mathbf{h}_{i,i,p(j)}\mathbf{w}_{i,p(j)}^{I,(\kappa)}\|^2 > 0, \qquad (50a) \\ &2\Re\{(\mathbf{w}_{i,p(j)}^{I,(\kappa)})^H\mathbf{h}_{i,i,j}^H\mathbf{h}_{i,i,j}\mathbf{w}_{i,p(j)}^I\} \\ &\quad -\|\mathbf{h}_{i,i,j}\mathbf{w}_{i,p(j)}^{I,(\kappa)}\|^2 > 0, \qquad (50b) \\ &2\Re\{(\mathbf{w}_{i,j}^{I,(\kappa)})^H\mathbf{h}_{i,i,j}^H\mathbf{h}_{i,i,j}\mathbf{w}_{i,j}^I\} \\ &\quad -\|\mathbf{h}_{i,i,j}\mathbf{w}_{i,j}^{I,(\kappa)}\|^2 > 0, \qquad (50c) \\ &\quad \text{for} \quad (i,j) \in \mathcal{I}\times\mathcal{J}_c. \end{aligned}$$

The EH constraint (46b) is innerly approximated by [7]

$$\sum_{(s,\ell)\in\mathcal{S}_c}\left[2\Re\left\{(\mathbf{w}_{s,\ell}^{E,(\kappa)})^H\mathbf{h}_{s,i,j}^H\mathbf{h}_{s,i,j}\mathbf{w}_{s,\ell}^E\right\} - \left|\mathbf{h}_{i,i,j}\mathbf{w}_{s,\ell}^{E,(\kappa)}\right|^2\right] + \sigma^2 \geq \frac{e_{i,j}^{\min}}{\zeta_{i,j}\rho}, \forall i\in\mathcal{I}, j\in\mathcal{J}_c \tag{51}$$

The power constraints (46d) is innerly approximated by [7]

$$\begin{aligned} &\frac{1}{1-\rho}\sum_{j\in\mathcal{J}_c}\|\mathbf{w}_{i,j}^E\|^2 + \sum_{j\in\mathcal{J}}\|\mathbf{w}_{i,j}^I\|^2 \leq \\ &\qquad \left(\frac{2}{1-\rho^{(\kappa)}} - \frac{1-\rho}{(1-\rho^{(\kappa)})^2}\right)P_i^{\max} \\ &+\sum_{j\in\mathcal{J}}\left(2\Re\left\{(\mathbf{w}_{i,j}^{E,(\kappa)})^H\mathbf{w}_{i,j}^E\right\} - \|\mathbf{w}_{i,j}^{E,(\kappa)}\|^2\right), \ \forall i\in\mathcal{I}. \end{aligned} \tag{52}$$

In summary, we propose to solve the following convex approximation at the κth iteration for $(\mathbf{w}^{E,(\kappa)}, \mathbf{w}^{I,(\kappa)}, \rho^{(\kappa)})$ found from the previous $(\kappa-1)$th iteration

$$\begin{aligned} &\max_{\rho,\mathbf{w}^E,\mathbf{w}^I} \min_{(i,j)\in\mathcal{I}\times\mathcal{J}} \mathcal{R}_{i,j} \\ &\text{s.t} \quad (46c),(46e),(46f),(47)-(49),(50),(51),(52). \end{aligned} \tag{53}$$

Algorithm 3 outlines the steps to solve the "transmit TS-based" algorithm for throughput max-min optimization problem (46). Like Algorithm 1, it converges at least to a local optimal solution satisfying the KKT condition. The initialization procedure will be stated shortly.

Algorithm 3 Transmit TS-based algorithm for throughput max-min optimization problem (46)

Initialization: Set $\kappa := 0$ and a feasible point $\mathbf{w}^{(0)} = (\mathbf{w}^{E,(0)}, \mathbf{w}^{I,(0)})$ and $\rho^{(0)}$ for constraints (46b)-(46f).
1: **repeat**
2: Solve the convex optimization problem (53) to obtain the optimal solution $(\mathbf{w}^{(\kappa+1)}, \rho^{(\kappa+1)})$.
3: Set $\kappa := \kappa + 1$.
4: **until** Convergence

Next, we address the following energy-efficiency maximization problem

$$\begin{aligned} &\max_{\mathbf{w},\mathcal{R},\rho} \frac{\sum_{(i,j)\in\mathcal{I}\times\mathcal{J}} \mathcal{R}_{i,j}}{\frac{1}{\xi}\left[\rho\pi_E(\mathbf{w}^E) + (1-\rho)\pi_I(\mathbf{w}^I)\right] + P_c} \\ &\quad \text{s.t.} \quad (20b),(20c),(46c),(46e), \\ &\qquad (46f),(43),(44),(45),(46b)-(46f) \end{aligned} \tag{54}$$

where ξ is the constant power amplifier efficiency, $P_c \triangleq N_tP_A + P_{\text{cir}}$, P_A is the power dissipation at each transmit antenna, P_{cir} is the fixed circuit power consumption for base-band processing,

$$\pi_E(\mathbf{w}^E) = \sum_{i\in\mathcal{I}}\sum_{j\in\mathcal{J}_c}\|\mathbf{w}_{i,j}^E\|^2$$

and

$$\pi_I(\mathbf{w}^I) = \sum_{i\in\mathcal{I}}\sum_{j\in\mathcal{J}}\|\mathbf{w}_{i,j}^I\|^2.$$

Note that we define $\rho\pi_E(\mathbf{w}^E) + (1-\rho)\pi_I(\mathbf{w}^I)$ to differentiate from $\pi(\mathbf{w})$ in (36). For this network, it is more appropriate to use $(1-\rho)\pi_I(\mathbf{w}^I)$ for information delivery.

Suppose $(\mathbf{w}^{(\kappa)}, \mathcal{R}^{(\kappa)}, \rho^{(\kappa)})$ is a feasible point for (54) that is found from the $(\kappa-1)$th iteration and

$$\begin{aligned} t^{(\kappa)} &= \frac{\sum_{(i,j)\in\mathcal{I}\times\mathcal{J}} \mathcal{R}_{i,j}^{(\kappa)}}{\frac{1}{\xi}\left[\rho^{(\kappa)}\pi_E(\mathbf{w}^{E,(\kappa)}) + (1-\rho^{(\kappa)})\pi_I(\mathbf{w}^{I,(\kappa)})\right] + P_c} \\ &= \frac{\sum_{(i,j)\in\mathcal{I}\times\mathcal{J}} \mathcal{R}_{i,j}^{(\kappa)}/(1-\rho^{(\kappa)})}{\frac{1}{\xi}\left(\frac{\pi_E(\mathbf{w}^{E,(\kappa)})}{(1-\rho^{(\kappa)})-1}\right) + \frac{1}{\xi}\pi_I(\mathbf{w}^{I,(\kappa)}) + \frac{P_c}{1-\rho^{(\kappa)}}} \end{aligned} \tag{55}$$

At the κth iteration we address the problem

$$\begin{aligned} &\max_{\mathbf{w},\mathcal{R},\rho} \frac{\sum_{(i,j)\in\mathcal{I}\times\mathcal{J}} \mathcal{R}_{i,j}}{1-\rho} \\ &\quad - t^{(\kappa)}\left[\frac{1}{\xi}\left(\frac{1}{1-\rho}-1\right)\pi_E(\mathbf{w}^E) + \frac{1}{\xi}\pi_I(\mathbf{w}^I) + \frac{P_c}{1-\rho}\right] \\ &\text{s.t.} \quad (20b),(20c),(46c),(46e),(46f),(43), \\ &\qquad (44),(45),(46b)-(46f). \end{aligned} \tag{56}$$

Substituting $x = \sum_{(i,j)\in\mathcal{I}\times\mathcal{J}} \mathcal{R}_{i,j}$, $\bar{x} = \sum_{(i,j)\in\mathcal{I}\times\mathcal{J}} \mathcal{R}_{i,j}^{(\kappa)}$, and $t = 1-\rho$, $\bar{t} = 1-\rho^{(\kappa)}$ to the following inequality

$$\frac{x}{t} \geq 2\frac{\sqrt{\bar{x}}}{\bar{t}}\sqrt{x} - \frac{\bar{x}}{\bar{t}^2}t \quad \forall\ x>0, \bar{x}>0, t>0, \bar{t}>0 \tag{57}$$

Algorithm 4 Transmit TS-based algorithm for energy-efficiency (EE) maximization problem (54)

Initialization: Set $\kappa := 0$ and a feasible point $(\mathbf{w}^{(0)}, \rho^{(0)})$ for (54) and also define $t^{(0)}$ by (55) for $\kappa = 0$.

1: **repeat**
2: Solve the convex optimization problem (60) to obtain the optimal solution $(\mathbf{w}^{(\kappa+1)}, \rho^{(\kappa+1)})$ and then define $t^{(\kappa+1)}$ by (55) (for $\kappa+1$).
3: Set $\kappa := \kappa + 1$.
4: **until** Convergence

whose proof is given by Appendix B, the first term in the objective of (56) is lower approximated by a concave function as

$$\frac{\sum\limits_{(i,j)\in\mathcal{I}\times\mathcal{J}} \mathcal{R}_{i,j}}{1-\rho} \geq f^{(\kappa)}(\mathcal{R},\rho) \triangleq 2\frac{\sqrt{\sum_{(i,j)\in\mathcal{I}\times\mathcal{J}} \mathcal{R}_{i,j}^{(\kappa)}}}{1-\rho^{(\kappa)}} \sqrt{\sum_{(i,j)\in\mathcal{I}\times\mathcal{J}} \mathcal{R}_{i,j}} - \frac{\sum_{(i,j)\in\mathcal{I}\times\mathcal{J}} \mathcal{R}_{i,j}^{(\kappa)}}{(1-\rho^{(\kappa)})^2}(1-\rho), \quad (58)$$

The second term in the objective of (56), i.e., $g(\mathbf{w},\rho) \triangleq \left[\frac{1}{\xi}\left(\frac{1}{1-\rho}-1\right)\pi_E(\mathbf{w}^E) + \frac{1}{\xi}\pi_I(\mathbf{w}^I) + \frac{P_c}{1-\rho}\right]$ is upper approximated by the convex function

$$g^{(\kappa)}(\mathbf{w},\rho) \triangleq \frac{1}{(1-\rho)}\frac{\pi_E(\mathbf{w}^E)}{\xi} + \frac{\pi_I(\mathbf{w}^I)}{\xi} + \frac{P_c}{1-\rho} - \frac{1}{\xi}\sum_{i\in\mathcal{I}}\sum_{j\in\mathcal{J}_c}\left(2\Re\{(\mathbf{w}_{i,j}^{E,(\kappa)})^H\mathbf{w}_{i,j}^E\} - \|\mathbf{w}_{i,j}^{E,(\kappa)}\|^2\right), \quad (59)$$

where we can easily obtain (59) by using the inequality

$$\|\mathbf{x}\|^2 \geq 2\Re\{(\mathbf{x}^{(\kappa)})^H\mathbf{x}\} - \|\mathbf{x}^{(\kappa)}\|^2$$

Thus, we solve the following convex optimization problem to generate $(\mathbf{w}^{(\kappa+1)}, \mathcal{R}^{(\kappa+1)}, \rho^{(\kappa+1)})$

$$\max_{\rho,\mathbf{w}^E,\mathbf{w}^I} \; [f^{(\kappa)}(\mathcal{R},\rho) - t^{(\kappa)}g^{(\kappa)}(\mathbf{w},\rho)]$$
$$\text{s.t} \quad (20b),(20c),(46c),(46e),(46f),(47)-(49),(50),(51),(52). \quad (60)$$

where $f^{(\kappa)}(\mathcal{R},\rho)$, $t^{(\kappa)}$, and $g^{(\kappa)}(\mathbf{w},\rho)$ are defined in (58), (55), and (59), respectively. Algorithm 4 outlines the steps to solve the "transmit-TS based" algorithm for the energy-efficiency (EE) maximization problem (54).

Generation of the initial points: A feasible point for initializing Algorithm 4 is found via the following iterations

$$\max_{\mathbf{w},\mathcal{R}} \min_{(i,j)\in\mathcal{I}\times\mathcal{J}_c} \left\{\frac{\mathcal{R}_{i,j}}{r_{i,j}} - 1, \frac{\mathcal{R}_{i,p(j)}}{r_{i,p(j)}} - 1, \zeta_{i,j}\sum_{(s,\ell)\in\mathcal{S}_c}\left(2\Re\{(\mathbf{w}_{s,\ell}^{E,(\kappa)})^H\mathbf{h}_{s,i,j}^H\mathbf{h}_{s,i,j}\mathbf{w}_{s,l}^E\} - |\mathbf{h}_{s,i,j}\mathbf{w}_{s,l}^{E,(\kappa)}|^2\right) + \zeta_{i,j}\sigma^2 - \frac{e_{i,j}^{\min}}{\rho^{(0)}}\right\}$$
$$\text{s.t.} \quad (46e),(46f), \quad (61a)$$
$$\rho^{(0)}\sum_{j\in\mathcal{J}_c}\|\mathbf{w}_{i,j}^E\|^2 + (1-\rho^{(0)})\sum_{j\in\mathcal{J}}\|\mathbf{w}_{i,j}^I\|^2 \leq P_i^{\max}, \quad (61b)$$
$$\frac{\mathcal{R}_{i,p(j)}}{1-\rho^{(0)}} \leq \Lambda_0(\mathbf{h}_{i,i,j}\mathbf{w}_{i,p(j)}^I, \mathcal{L}_{i,p(j)}^c(\mathbf{w}^I)), \quad (61c)$$
$$\frac{\mathcal{R}_{i,p(j)}}{1-\rho^{(0)}} \leq \Lambda_0(\mathbf{h}_{i,i,p(j)}\mathbf{w}_{i,p(j)}^I, \mathcal{L}_{i,p(j)}^e(\mathbf{w}^I)), \quad (61d)$$
$$\frac{\mathcal{R}_{i,j}}{1-\rho^{(0)}} \leq \Lambda_0(\mathbf{h}_{i,i,j}\mathbf{w}_{i,j}^I, \mathcal{L}_{i,j}^c(\mathbf{w}^I)), \quad (61e)$$

till reaching a value more than or equal to 0, for a fixed $\rho^{(0)}$.

A good feasible point for initializing Algorithm 3 can also be found from (61) by setting before hand good values of $r_{i,j}$.

IV. Simulation Results

To analyze the proposed algorithms through simulations, a network topology as shown in Fig. 2 is set up. There are $N = 3$ cells and $2K = 4$ UEs per cell with two placed close to the BS and the remaining two placed near cell-edges. The cell radius is set to be 100 meters, where, near-by users are placed about the distance of 10 meters from the serving BS while cell-edge users are placed about the distance of $80-90$ meters from the serving BS. The channel $\mathbf{h}_{s,i,j}$ from BS $s \in \mathcal{I}$ to UE (i,j) at a distance of d meters is generated as $\mathbf{h}_{s,i,j} = \sqrt{10^{-\sigma_{\text{PL}}/10}}\tilde{\mathbf{h}}_{s,i,j}$, where $\sigma_{\text{PL}} = 30 + 10\beta\log_{10}(d)$ is the path-loss in dB (the path-loss model is consistent with dense user deployment settings and wireless energy harvesting requirements [26]), β is the path-loss exponent, and $\tilde{\mathbf{h}}_{s,i,j}$ is the normalized Rayleigh fading channel gain (for $s = i$ while $j \in \mathcal{J}_e$ or $s \neq i$, i.e., channel between BS and its own cell-edge users or channel between BS and users in the neigboring cells) or $\tilde{\mathbf{h}}_{s,i,j}$ is the Rician fading channel gain with Rician factor of 10 dB (for $s = i$ while $j \in \mathcal{J}_c$, i.e., channel between BS and its own cell-centered users). We set the path-loss exponents $\beta = 3$ for the former case and $\beta = 2$ for the later case. Different values for path-loss exponents have been proposed for different type of users in the literature too [38], [39]. For simplicity, set $e_{i,j}^{\min} \equiv e^{\min}$ for the energy harvesting thresholds, $\zeta_{i,j} \equiv \zeta$, $\forall i,j$ for the energy harvesting conversion, $P_i^{\max} \equiv P^{\max}$, $\forall\, i$. Further, we set the energy harvesting threshold $e^{\min} = -20$ dBm and energy conversion efficiency $\zeta = 0.5$, $P^{\max} = -35$ dBm (unless stated otherwise), noise variances $\sigma^2 = \sigma_c^2 = -174$ dBm/Hz (unless stated otherwise), bandwidth = 20 MHz,

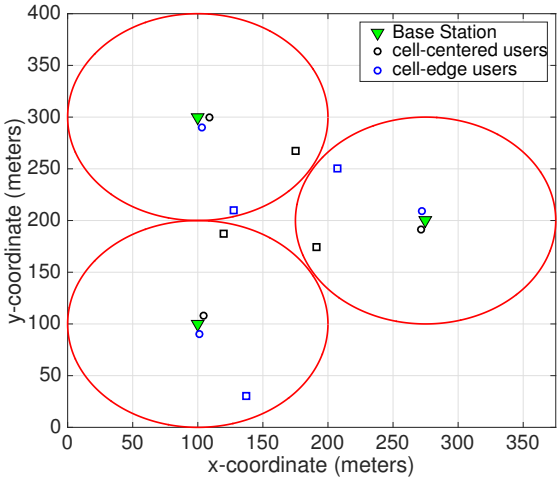

Fig. 2. A multicell network setup used in our numerical examples.

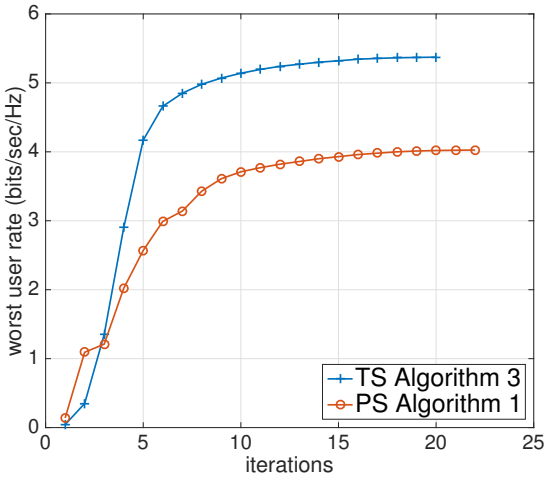

Fig. 3. Convergence of PS-based Algorithm 1 and TS-based Algorithm 3 for $M = 6$ and $P^{\max} = -35$ dBm.

and carrier frequency = 2 GHz. For energy efficiency maximization problems (20) and (54), we set the threshold rate $r_{i,j} = 0.5$ bits/sec/Hz $\forall\ i, j$ (unless stated otherwise), we choose the power amplifier efficiency $\xi = 0.2$, power dissipation at each transmit antenna $P_A = 0.6$W (27.78 dBm), and circuit power consumption $P_{\text{cir}} = 2.5$W (33.97 dBm) [40], [41]. .

A. Results for throughput max-min optimization problems (19) *and* (46)*:*

Fig. 3 shows the convergence of the PS-based Algorithm 1 and the TS-based Algorithm 3, which aim to solve the throughput max-min optimization problems (19) and (46), respectively. The simulation in Fig. 3 assumes $M = 6$ antennas at the BS and transmit power budget $P^{\max} = -35$ dBm. We can see that under some fixed channel realization, both algorithms converge within 15-20 observations, approximately, while TS-based Algorithm 3 achieves higher max-min rate compared to that achieved by PS-based Algorithm 1. On average (running 100 simulations and averaging over random channel realizations), we observe that the PS-based Algorithm 1 requires 15.65 iterations, while TS-based Algorithm 3 requires 18.7 iterations before convergence.

Fig. 4 plots the optimized max-min rate for varying number of BS-antennas and fixed BS power budget $P^{\max} = 35$ dBm, while solving the power splitting (PS)-based problem (19) and time switching (TS)-based problem (46). As expected, the rate increases by increasing the number of antennas at the BS. We can also observe from Fig. 4 that the TS-based Algorithm 3 outperforms the PS-based Algorithm 1 in terms of achievable rate and the corresponding performance gap increases if we increase the number of antennas mounted on the BS. Fig. 5 plots the optimized worst user rate for varying values of BS transmit power budget $P^{\max}$ and fixed number of BS-antennas $M = 6$, while solving the same power splitting (PS)-based problem (19) and time switching (TS)-based problem (46). Fig. 5 shows that increasing the transmit power budget raises the level of achievable rate, however, the increase diminishes at higher values of transmit power budget, e.g., we can see marginal improvement in the rate when we increase the transmit power budget from $P^{\max} = 43$ dBm to 45 dBm. Similar to previous result in Fig. 4, we observe from Fig. 5 that the TS-based Algorithm 3 outperforms the PS-based Algorithm 1 in terms of achievable rate. Fig. 6 plots the optimized worst user rate for varying values of noise variances σ^2 (in dBm/Hz) and fixed value of transmit power budget $P^{\max} = 35$ dBm and BS antennas $M = 6$, while solving the same power splitting (PS)-based problem (19) and time switching (TS)-based problem (46). Fig. 6 shows that, as expected, increasing the noise variance decreases the level of achievable rate. However, we observe a minor decrease in the achievable rate for PS-based receiver. Therefore, though the TS-based Algorithm 3 outperforms the PS-based Algorithm 1 in terms of achievable rate, but the corresponding performance gap decreases if we increase the noise variance.

B. Results for energy efficiency maximization problems (20) *and* (54)*:*

Fig. 7 shows the convergence of the PS-based Algorithm 2 and TS-based Algorithm 4, which aim to solve the energy efficiency maximization problems (20) and (54), respectively. The simulation in Fig. 7 assumes $M = 4$ antennas at the BS and transmit power budget $P^{\max} = -35$ dBm. We can see that under some fixed channel realization, both algorithms converge within 10-15 observations, approximately, while the TS-based Algorithm 4 achieves a higher energy efficiency compared to that achieved by

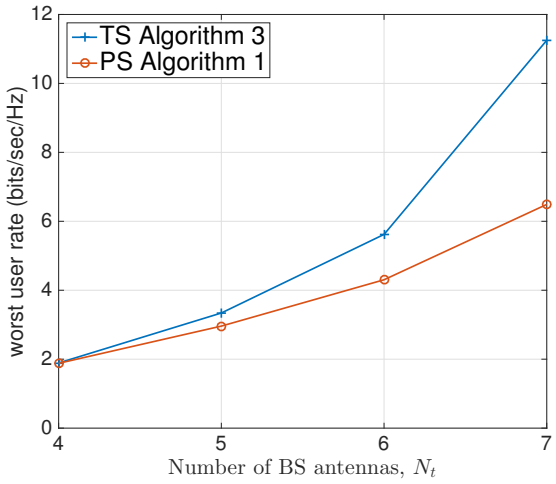

Fig. 4. Optimized worst user rate for varying number of antennas and fixed BS power budget $P^{\max} = 35$ dBm, while solving power splitting (PS)-based problem (19) and time switching (TS)-based problem (46).

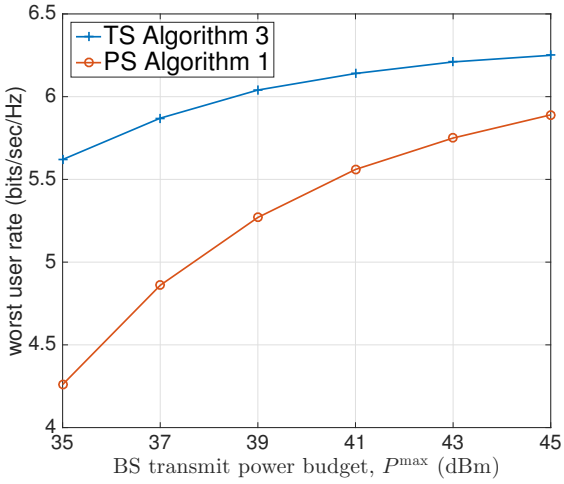

Fig. 5. Optimized worst user rate for varying values of BS transmit power budget $P^{\max}$ and fixed value of $M = 6$, while solving power splitting (PS)-based problem (19) and time switching (TS)-based problem (46).

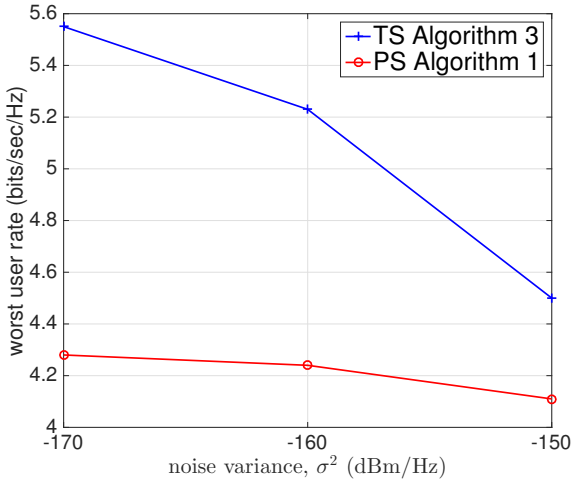

Fig. 6. Optimized worst user rate for varying values of noise variances σ^2 and fixed value of $P^{\max} = 35$ dBm and BS antennas $M = 6$, while solving power splitting (PS)-based problem (19) and time switching (TS)-based problem (46).

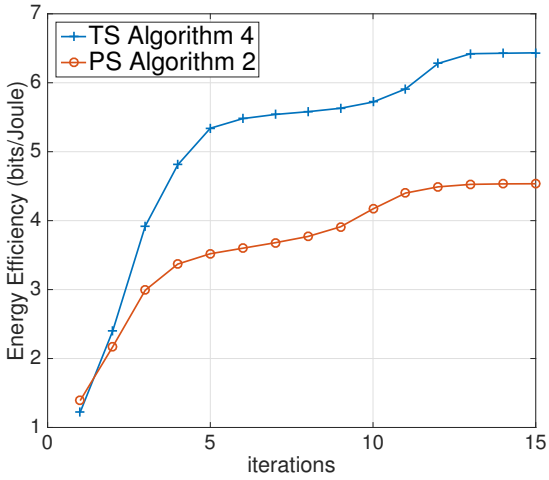

Fig. 7. Convergence of PS-based Algorithm 2 and TS-based Algorithm 4 for $M = 4$ and $P^{\max} = -35$ dBm.

the PS-based Algorithm 2. On average (running 100 simulations and averaging over random channel realizations), we observe that the PS-based Algorithm 2 requires 13.25 iterations, while the TS-based Algorithm 4 requires 15.9 iterations before convergence.

Fig. 8 plots the optimized energy efficiency (EE) for a varying number of BS-antennas and fixed BS power budget $P^{\max} = 35$ dBm, while solving power splitting (PS)-based problem (20) and time switching (TS)-based problem (54). As expected, the EE increases by increasing the number of antennas at the BS. We can also observe from Fig. 8 that the TS-based Algorithm 4 outperforms the PS-based Algorithm 2 in terms of achievable EE and the performance gap is more than 1 bit/Joule. Next, Fig. 9 plots the energy efficiency for varying values of BS transmit power budget $P^{\max}$ and fixed number of BS-antennas $M = 4$, while solving the same power splitting (PS)-based problem (20) and time switching (TS)-based problem (54). Fig. 9 shows that for TS-based implementation, increasing the transmit power budget raises the level of achievable EE, however, for PS-based implementation, there is almost no improvement in EE when the transmit power budget is increased from $P^{\max} = 35$ dBm to 45 dBm.

Fig. 10 plots the optimized energy efficiency for different values of noise variances σ^2 (in dBm/Hz) and fixed value of transmit power budget $P^{\max} = 35$ dBm and BS antennas

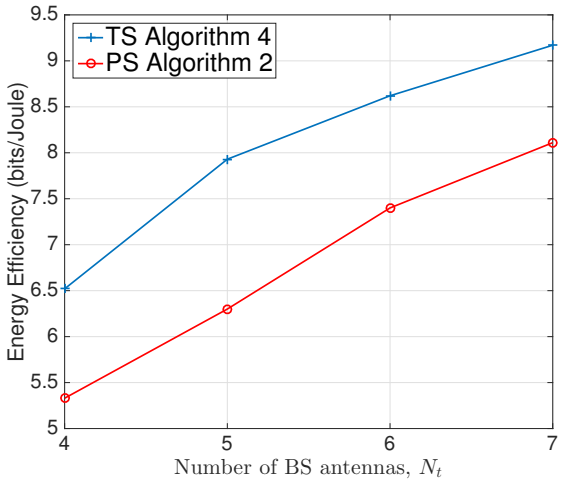

Fig. 8. Optimized energy efficiency for varying number of antennas and fixed BS power budget $P^{\max} = 35$ dBm, while solving power splitting (PS)-based problem (20) and time switching (TS)-based problem (54).

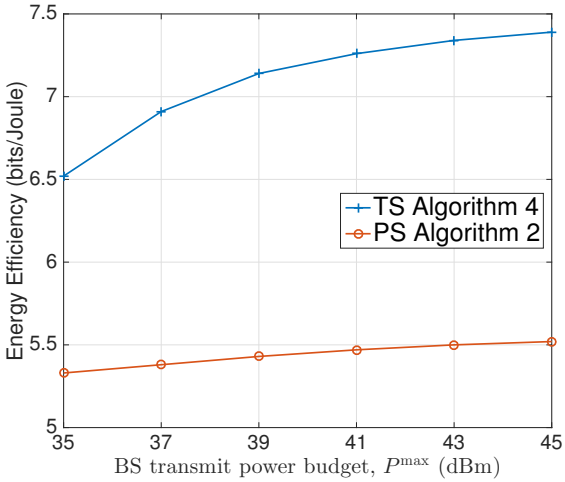

Fig. 9. Optimized energy efficiency for varying values of noise variances σ^2 and fixed BS transmit power budget $P^{\max} = 35$ and fixed value of $M = 4$, while solving power splitting (PS)-based problem (20) and time switching (TS)-based problem (54)

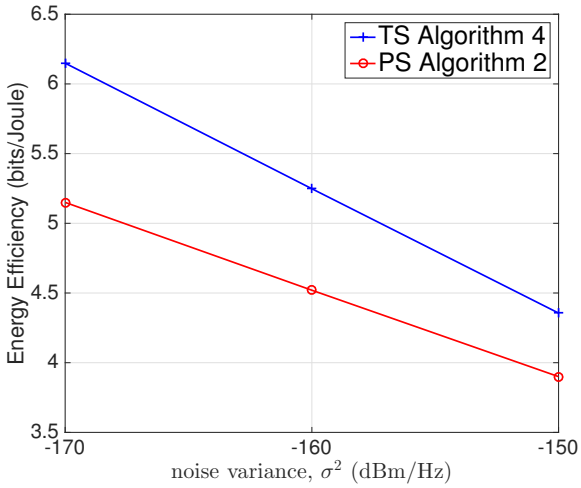

Fig. 10. Optimized energy efficiency for varying values of of noise variances σ^2 and fixed value of $P^{\max} = 35$ dBm and BS antennas $M = 4$, while solving power splitting (PS)-based problem (20) and time switching (TS)-based problem (54)

$M = 4$, while solving the power splitting (PS)-based problem (20) and time switching (TS)-based problem (54). Fig. 10 shows that, as expected, EE decreases by increasing the noise variance. In addition, the TS-based Algorithm 4 outperforms the PS-based Algorithm 2 in terms of EE. Nevertheless, this performance gap decreases with the increase of noise variance.

C. Comparison with orthogonal multiple access (OMA):

Fig. 11 plots the optimized worst user rate for varying values of BS transmit power budget $P^{\max}$ and fixed number of BS-antennas $M = 6$, while solving same power splitting (PS)-based NOMA problem (19), time switching (TS)-based NOMA problem (46), and their orthogonal multiple access (OMA) counterparts. In parallel, Fig. 12 plots the energy efficiency for varying values of BS transmit power budget $P^{\max}$ and fixed number of BS-antennas $M = 4$ and threshold rate $r_{i,j} = 0.1$ bits/sec/Hz (different from previous EE plots), while solving the power splitting (PS)-based NOMA problem (20), time switching (TS)-based NOMA problem (54), and their OMA counterparts. We have to choose a smaller threshold rate $r_{i,j} = 0.1$ bits/sec/Hz because implementation with OMA scheme fails to simultaneously satisfy both the higher threshold rate and the EH constraint *for all simulations*. We can clearly observe from Figs. 11 and 12 that NOMA implementation outperforms OMA implementation, in terms of both, throughput and energy efficiency, respectively.

V. Conclusions

In this paper, we have considered energy harvesting based NOMA system, where transmit-TS approach is employed to realize wireless energy harvesting and information decoding at the nearly-located users. We have formulated two important problems of worst-user throughput maximization and energy efficiency maximization under power constraint and energy harvesting constraints at the nearly-located users. For these problems, the optimization objective and energy harvesting constraints are highly non-convex. To address this, we have developed efficient path-following algorithms to solve the two problems. We have also proposed algorithms for the case if conventional PS-based approach is used for energy harvesting. Our numerical results confirmed that the proposed transmit-TS approach clearly outperforms PS approach in terms of both, throughput and energy efficiency.

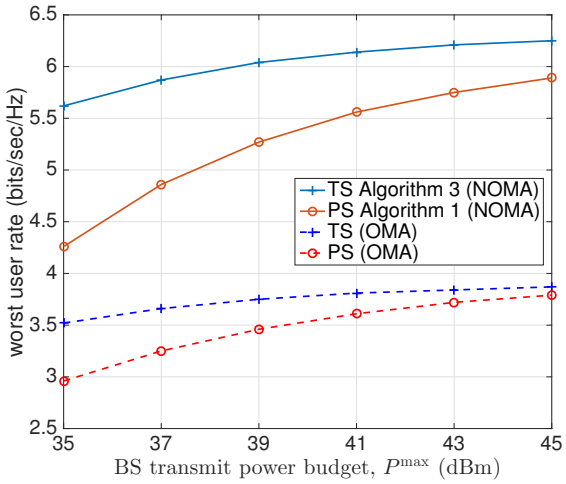

Fig. 11. Optimized worst user rate for varying values of BS transmit power budget $P^{\max}$ and fixed value of $M = 6$, while solving power splitting (PS)-based NOMA problem (19), time switching (TS)-based NOMA problem (46), and their OMA counterparts.

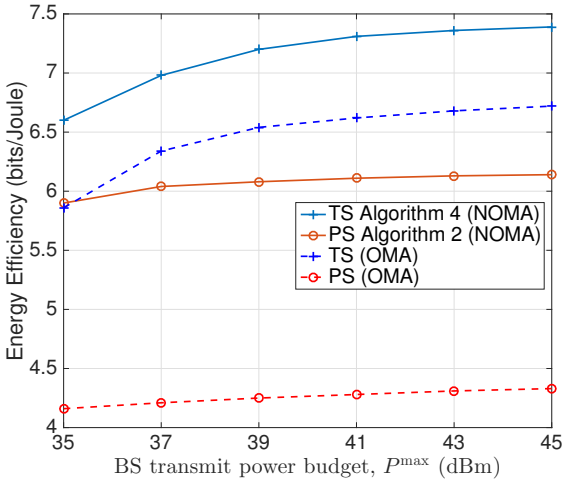

Fig. 12. Optimized energy efficiency for varying values of BS transmit power budget $P^{\max}$ and fixed value of $M = 4$ and threshold rate $r_{i,j} = 0.1$ bits/sec/Hz (different from previous EE plots), while solving power splitting (PS)-based NOMA problem (20), time switching (TS)-based NOMA problem (54), and their OMA counterparts.

Appendix A: Proof for (21)-(24)

Define function $f(x,y) \triangleq \ln(x^{-1}+y^{-1})$ which is convex in $x>0$ and $y>0$ [42]. Next, by using the following inequality $\forall\ x>0,\ y>0,\ x^{(\kappa)}>0,\ y^{(\kappa)}>0$ [43]

$$\begin{aligned}\ln\left(\frac{1}{x}+\frac{1}{y}\right) &\geq f(x^{(\kappa)},y^{(\kappa)}) \\ &\quad +\langle\nabla f(x^{(\kappa)},y^{(\kappa)}),(x,y)-(x^{(\kappa)},y^{(\kappa)})\rangle \\ &= \ln\left(\frac{1}{x^{(\kappa)}}+\frac{1}{y^{(\kappa)}}\right)+1 \\ &\quad -\frac{1}{x^{(\kappa)}+y^{(\kappa)}}\left(\frac{y^{(\kappa)}}{x^{(\kappa)}}x+\frac{x^{(\kappa)}}{y^{(\kappa)}}y\right) \end{aligned} \quad (62)$$

Substituting $x=\|\mathbf{x}\|^2$, $y=\|\mathbf{y}\|^2+\sigma^2$, $x^{(\kappa)}=\|\mathbf{x}^{(\kappa)}\|^2$, and $y^{(\kappa)}=\|\mathbf{y}^{(\kappa)}\|^2+\sigma^2$, we have

$$\begin{aligned}&\ln\left((\|\mathbf{x}\|^2)^{-1}+(\|\mathbf{y}\|^2+\sigma^2)^{-1}\right) \geq \\ &\ln\left((\|\mathbf{x}^{(\kappa)}\|^2)^{-1}+(\|\mathbf{y}^{(\kappa)}\|^2+\sigma^2)^{-1}\right)+1 \\ &-\frac{1}{\|\mathbf{x}^{(\kappa)}\|^2+\|\mathbf{y}^{(\kappa)}\|^2+\sigma^2}\left(\frac{\|\mathbf{y}^{(\kappa)}\|^2+\sigma^2}{\|\mathbf{x}^{(\kappa)}\|^2}\|\mathbf{x}\|^2\right. \\ &\left.+\frac{\|\mathbf{x}^{(\kappa)}\|^2}{\|\mathbf{y}^{(\kappa)}\|^2+\sigma^2}(\|\mathbf{y}\|^2+\sigma^2)\right). \end{aligned} \quad (63)$$

Next, as functions $\ln(1/x)$ and $\|\mathbf{x}\|^2$ are convex, it is true that

$$\ln\left(\frac{1}{x}\right) \geq \ln\left(\frac{1}{x^{(\kappa)}}\right)-\frac{x-x^{(\kappa)}}{x^{(\kappa)}} \quad (64)$$

$$\|\mathbf{x}\|^2 \geq 2\Re\{(\mathbf{x}^{(\kappa)})^H\mathbf{x}\}-\|\mathbf{x}^{(\kappa)}\|^2. \quad (65)$$

By substituting $\|\mathbf{x}\|^2$ and $\|\mathbf{x}^{(\kappa)}\|^2$ in place of $\frac{1}{x}$ and $\frac{1}{x^{(\kappa)}}$ in (64), we have the following inequality:

$$\ln(\|\mathbf{x}\|^2) \geq \ln(\|\mathbf{x}^{(\kappa)}\|^2)+1-\frac{\|\mathbf{x}^{(\kappa)}\|^2}{2\Re\{(\mathbf{x}^{(\kappa)})^H\mathbf{x}\}-\|\mathbf{x}^{(\kappa)}\|^2} \quad (66)$$

over the trust region (23). Combining (63) and (66) leads to (21)-(22).

Note that it is straightforward to prove (24) by simply substituting $\mathbf{x}=\mathbf{x}^{(\kappa)}$ and $\mathbf{y}=\mathbf{y}^{(\kappa)}$ in (21).

Appendix B: Proof for (57)

As function $g(x,t) \triangleq x^2/t$ is convex in $x>0$ and $t>0$, it is true that [43]

$$\begin{aligned}\frac{x^2}{t} &\geq g(\bar{x},\bar{t})+\langle\nabla g(\bar{x},\bar{t}),(x,t)-(\bar{x},\bar{t})\rangle \\ &= 2\frac{\bar{x}}{\bar{t}}x-\frac{\bar{x}^2}{\bar{t}^2}t. \end{aligned} \quad (67)$$

Inequality (57) then follows by resetting $x \to \sqrt{x}$ and $\bar{x} \to \sqrt{\bar{x}}$.

References

[1] X. Lu, P. Wang, D. Niyato, D. I. Kim, and Z. Han, "Wireless networks with RF energy harvesting: A contemporary survey," *IEEE Commun. Surveys Tuts.*, vol. 17, pp. 757–789, 2015.

[2] A. A. Nasir, H. D. Tuan, D. T. Ngo, S. Durrani, and D. I. Kim, "Path-following algorithms for beamforming and signal splitting in RF energy harvesting networks," *IEEE Commun. Letters*, vol. 20, no. 8, pp. 1687–1690, Aug 2016.

[3] V. D. Nguyen, T. Q. Duong, H. D. Tuan, O. S. Shin, and H. V. Poor, "Spectral and energy efficiencies in full-duplex wireless information and power transfer," *IEEE Trans. Commun.*, vol. 65, no. 5, pp. 2220–2233, May 2017.

[4] H. H. M. Tam, H. D. Tuan, A. A. Nasir, T. Q. Duong, and H. V. Poor, "MIMO energy harvesting in full-duplex multi-user networks," *IEEE Trans. Wireless Commun.*, vol. 16, no. 5, pp. 3282–3297, May 2017.

[5] A. A. Nasir, H. D. Tuan, T. Q. Duong, and H. V. Poor, "Secrecy rate beamforming for multicell networks with information and energy harvesting," *IEEE Trans. Signal Process.*, vol. 65, no. 3, pp. 677–689, 2017.

[6] A. A. Nasir, H. D. Tuan, D. T. Ngo, T. Q. Duong, and H. V. Poor, "Beamforming design for wireless information and power transfer systems: Receive power-splitting vs transmit time-switching," *IEEE Trans. Commun.*, vol. 65, no. 2, pp. 876–889, 2017.

[7] A. A. Nasir, H. D. Tuan, T. Q. Duong, and H. V. Poor, "Secure and energy-efficient beamforming for simultaneous information and energy transfer," *IEEE Trans. Wireless Commun.*, vol. 16, no. 11, pp. 7523–7537, Nov 2017.

[8] Y. Saito, Y. Kishiyama, A. Benjebbour, T. Nakamura, A. Li, and K. Higuchi, "Non-orthogonal multiple access (NOMA) for cellular future radio access," in *Proc. IEEE Veh. Technol. Conf. (VTC Spring)*, June 2013, pp. 1–5.

[9] W. Shin, M. Vaezi, B. Lee, D. J. Love, J. Lee, and H. V. Poor, "Non-orthogonal multiple access in multi-cell networks: Theory, performance, and practical challenges," *IEEE Commun. Mag.*, vol. 55, no. 10, pp. 176–183, Oct. 2017.

[10] V. D. Nguyen, H. D. Tuan, T. Q. Duong, H. V. Poor, and O. S. Shin, "Precoder design for signal superposition in MIMO-NOMA multicell networks," *IEEE J. Select. Areas Commun.*, vol. 35, no. 12, pp. 2681–2695, Dec 2017.

[11] P. D. Diamantoulakis, K. N. Pappi, Z. Ding, and G. K. Karagiannidis, "Wireless-powered communications with non-orthogonal multiple access," *IEEE Trans. Wireless Commun.*, vol. 15, no. 12, pp. 8422–8436, Dec 2016.

[12] H. Chingoska, Z. Hadzi-Velkov, I. Nikoloska, and N. Zlatanov, "Resource allocation in wireless powered communication networks with non-orthogonal multiple access," *IEEE Wireless Commun. Lett.*, vol. 5, no. 6, pp. 684–687, Dec 2016.

[13] M. Song and M. Zheng, "Energy efficiency optimization for wireless powered sensor networks with non-orthogonal multiple access," *IEEE Sensors Letters*, vol. PP, no. 99, pp. 1–1, 2018.

[14] M. Moltafet, P. Azmi, N. Mokari, M. R. Javan, and A. Mokdad, "Optimal and fair energy efficient resource allocation for energy harvesting enabled-PD-NOMA based hetnets," *IEEE Trans. Wireless Commun.*, vol. PP, no. 99, pp. 1–1, 2018.

[15] Y. Wang, Y. Wu, F. Zhou, Z. Chu, Y. Wu, and F. Yuan, "Multi-objective resource allocation in a NOMA cognitive radio network with a practical non-linear energy harvesting model," *IEEE Access*, vol. PP, no. 99, pp. 1–1, 2017.

[16] Z. Yang, Y. Pan, W. Xu, R. Guan, Y. Wang, and M. Chen, "Energy efficient resource allocation for machine-to-machine communications with NOMA and energy harvesting," in *Proc IEEE INFOCOM*, May 2017, pp. 145–150.

[17] Z. Yang, W. Xu, Y. Pan, C. Pan, and M. Chen, "Energy efficient resource allocation in machine-to-machine communications with multiple access and energy harvesting for IoT," *IEEE Internet of Things J.*, vol. PP, no. 99, pp. 1–1, 2017.

[18] M. Ashraf, A. Shahid, J. W. Jang, and K. G. Lee, "Energy harvesting non-orthogonal multiple access system with multi-antenna relay and base station," *IEEE Access*, vol. 5, pp. 17 660–17 670, 2017.

[19] W. Han, J. Ge, and J. Men, "Performance analysis for NOMA energy harvesting relaying networks with transmit antenna selection and maximal-ratio combining over nakagami-m fading," *IET Communications*, vol. 10, no. 18, pp. 2687–2693, 2016.

[20] D.-B. Ha and S. Q. Nguyen, "Outage performance of energy harvesting DF relaying NOMA networks," *Mobile Networks and Applications*, Oct 2017. [Online]. Available: https://doi.org/10.1007/s11036-017-0922-x

[21] Y. Liu, Z. Ding, M. Elkashlan, and H. V. Poor, "Cooperative non-orthogonal multiple access with simultaneous wireless information and power transfer," *IEEE J. Select. Areas Commun.*, vol. 34, no. 4, pp. 938–953, April 2016.

[22] Y. Xu, C. Shen, Z. Ding, X. Sun, S. Yan, G. Zhu, and Z. Zhong, "Joint beamforming and power-splitting control in downlink cooperative SWIPT NOMA systems," *IEEE Trans. Signal Process.*, vol. 65, no. 18, pp. 4874–4886, Sept. 2017.

[23] Z. Yang, Z. Ding, P. Fan, and N. Al-Dhahir, "The impact of power allocation on cooperative non-orthogonal multiple access networks with swipt," *IEEE Trans. Wireless Commun.*, vol. 16, no. 7, pp. 4332–4343, July 2017.

[24] R. Sun, Y. Wang, X. Wang, and Y. Zhang, "Transceiver design for cooperative non-orthogonal multiple access systems with wireless energy transfer," *IET Communications*, vol. 10, no. 15, pp. 1947–1955, 2016.

[25] Y. Zhang, J. Ge, and E. Serpedin, "Performance analysis of a 5G energy-constrained downlink relaying network with non-orthogonal multiple access," *IEEE Trans. Wireless Commun.*, vol. 16, no. 12, pp. 8333–8346, Dec 2017.

[26] T. N. Do, D. B. da Costa, T. Q. Duong, and B. An, "Improving the performance of cell-edge users in MISO-NOMA systems using TAS and SWIPT-based cooperative transmissions," *IEEE Trans. Green Commun. Netw.*, vol. PP, no. 99, pp. 1–1, 2017.

[27] W. Guo and Y. Wang, "Cooperative non-orthogonal multiple access with energy harvesting," *Information*, vol. 8, no. 3, 2017.

[28] J. Gong and X. Chen, "Achievable rate region of non-orthogonal multiple access systems with wireless powered decoder," *IEEE J. Select. Areas Commun.*, vol. 35, no. 12, pp. 2846–2859, Dec 2017.

[29] G. He, L. Li, X. Li, W. Chen, L. L. Yang, and Z. Han, "Secrecy sum rate maximization in NOMA systems with wireless information and power transfer," in *Proc IEEE Int. Conf. Wirel. Commun. Signal Process. (WCSP)*, Oct 2017, pp. 1–6.

[30] A. H. Phan, H. D. Tuan, H. H. Kha, and D. T. Ngo, "Nonsmooth optimization for efficient beamforming in cognitive radio multicast transmission," vol. 60, no. 6, pp. 2941–2951, Jun. 2012.

[31] R. L. G. Cavalcante, S. Stanczak, M. Schubert, A. Eisenlatter, and U. Turke, "Toward energy-efficienct 5G wireless communications technologies," *IEEE Signal Process. Magazine*, vol. 13, no. 11, pp. 24–34, Nov. 2014.

[32] Z. Ding, P. Fan, and H. V. Poor, "Impact of user pairing on 5G nonorthogonal multiple-access downlink transmissions," *IEEE Trans. Veh. Technol.*, vol. 65, no. 8, pp. 6010–6023, Aug. 2016.

[33] Y. Liu, M. Elkashlan, Z. Ding, and G. K. Karagiannidis, "Fairness of user clustering in MIMO non-orthogonal multiple access systems," *IEEE Commun. Lett.*, vol. 20, no. 7, pp. 1465–1468, July 2016.

[34] B. Clerckx and E. Bayguzina, "Waveform design for wireless power transfer," *IEEE Trans. Signal Process.*, vol. 64, no. 23, pp. 6313–6328, Dec 2016.

[35] B. Clerckx, "Wireless information and power transfer: Nonlinearity, waveform design, and rate-energy tradeoff," *IEEE Trans. Signal Process.*, vol. 66, no. 4, pp. 847–862, Feb 2018.

[36] S. Buzzi, C. L. I, T. E. Klein, H. V. Poor, C. Yang, and A. Zappone, "A survey of energy-efficient techniques for 5G networks and challenges ahead," *IEEE J. Select. Areas Commun.*, vol. 34, no. 4, pp. 697–709, April 2016.

[37] Z. Sheng, H. D. Tuan, A. A. Nasir, T. Q. Duong, and H. V. Poor, "Power allocation for energy efficiency and secrecy of interference wireless networks," 2017. [Online]. Available: https://arxiv.org/pdf/1708.07334.pdf

[38] Y. Liu, Z. Qin, M. Elkashlan, A. Nallanathan, and J. A. McCann, "Non-orthogonal multiple access in large-scale heterogeneous networks," *IEEE J. Select. Areas Commun.*, vol. 35, no. 12, pp. 2667–2680, Dec 2017.

[39] A. Ghazanfari, H. Tabassum, and E. Hossain, "Ambient RF energy harvesting in ultra-dense small cell networks: performance and trade-offs," *IEEE Wireless Communications*, vol. 23, no. 2, pp. 38–45, April 2016.

[40] M. Imran, E. Katranaras, G. Auer, O. Blume, V. Giannini, Y. J. I. Godor, M. Olsson, D. Sabella, P. Skillermark, and W. Wajda, "Analysis of the reference systems, areas of improvements and target breakdown," *EARTH Project Deliverable D*, vol. 2, Jun 2011.

[41] S. Leng, D. W. K. Ng, N. Zlatanov, and R. Schober, "Multi-objective beamforming for energy-efficient SWIPT systems," in *Proc IEEE ICNC*, Feb 2016, pp. 1–7.

[42] H. M. T. Ho, H. D. Tuan, D. T. Ngo, T. Q. Duong, and H. V. Poor, "Joint load balancing and interference management for small-cell heterogeneous networks with limited backhaul capacity," *IEEE Trans. Wireless Commun.*, vol. 16, no. 2, pp. 872–884, Feb. 2017.

[43] H. Tuy, *Convex Analysis and Global Optimization (second edition)*. Springer, 2016.